Published in final edited form as:

Nat Cell Biol. 2015 April ; 17(4): 458–469. doi:10.1038/ncb3132.

The telomere bouquet regulates meiotic centromere assembly

Michael Klutstein[1,2,3], **Alex Fennell**[1,2], **Alfonso Fernández-Álvarez**[1,2], **Julia Promisel Cooper**[1,2,4]

[1]National Cancer Institute, NIH, Bethesda, Maryland 20892, USA.

[2]Cancer Research UK, London Research Institute, London WC2A 3LY, UK.

[3]Present address: Institute of Medical Research Israel-Canada, Hebrew University Medical School, Ein Kerem, Jerusalem 9112102, Israel.

Abstract

The role of the conserved meiotic telomere bouquet has been enigmatic for over a century. We showed previously that disruption of the fission yeast bouquet impairs spindle formation in approximately half of meiotic cells. Surprisingly, bouquet-deficient meiocytes with functional spindles harbour chromosomes that fail to achieve spindle attachment. Kinetochore proteins and the centromeric histone H3 variant Cnp1 fail to localize to those centromeres that exhibit spindle attachment defects in the bouquet's absence. The HP1 orthologue Swi6 also fails to bind these centromeres, suggesting that compromised pericentromeric heterochromatin underlies the kinetochore defects. We find that centromeres are prone to disassembly during meiosis, but this is reversed by localization of centromeres to the telomere-proximal microenvironment, which is conducive to heterochromatin formation and centromere reassembly. Accordingly, artificially tethering a centromere to a telomere rescues the tethered centromere but not other centromeres. These results reveal an unanticipated level of control of centromeres by telomeres.

Numerous principles of chromosome recombination and cell cycle control have been illuminated by studying meiosis, the specialized cell division cycle in which mating-competent haploid gametes are generated from diploid progenitors. Meiosis consists of two consecutive nuclear divisions, meiosis I and II (MI and MII), after one round of DNA replication. In MI, pairs of homologous chromosomes, one derived from each parent, segregate from each other having undergone homologous recombination; in MII, the sister chromatids within each homologous chromosome separate, leading to genome haploidization. MI is preceded by a lengthy prophase stage during which the homologues need to find each other and pair[1]. Hence, prophase involves marked chromosome

[4]Correspondence should be addressed to J.P.C. (Julie.Cooper@nih.gov).

AUTHOR CONTRIBUTIONS

J.P.C., M.K. and A.F. designed the study. M.K. performed experiments for nearly all figures. A.F. performed the experiments in Fig. 5a and helped with experiments in Figs 3 and 6 as well as strain construction and data analysis throughout. A.F-A. performed the experiments in Figs 6c and 8 and analysis of cells with nuclear membrane markers (Supplementary Videos 3 and 4), and helped with strain construction and data analysis. J.P.C. supervised the study. J.P.C. and M.K. wrote the manuscript and all authors edited it.

Supplementary Information is available in the online version of the paper

COMPETING FINANCIAL INTERESTS

The authors declare no competing financial interests.

movements. Chief among these is formation of the highly conserved telomere bouquet, in which telomeres gather at the nuclear periphery, often close to the centrosome.

Fission yeast has an especially striking and lengthy bouquet stage, allowing definition of the mechanistic underpinnings and functions of the bouquet. The fission yeast bouquet forms at the nuclear membrane just underneath the centrosome (called the spindle pole body or SPB) to which it is connected through a transmembrane linkage comprising a conserved SUN–KASH protein pair. On meiotic induction, the meiotic prophase-specific proteins Bqt1 and Bqt2 bind the telomeric Rap1 and Taz1 proteins (orthologues of human RAP1, TRF1 and TRF2) and connect telomeres with the SUN-domain protein Sad1 (refs 2–6); the resulting telomere–Bqt1/2–SUN–KASH–SPB bridge thus formed constitutes the bouquet and persists throughout prophase. Deletion of the genes encoding Bqt1, Bqt2, Rap1 or Taz1 dismantles the bouquet and, by confounding the directed chromosome movements required for homologue alignment, disrupts meiotic recombination[4,7–11]. Moreover, we showed previously that the bouquet has a crucial function in controlling the behaviour of the SPB and promoting spindle formation[12].

The clustering of telomeres within the bouquet also brings about clustering of the telomere-associated heterochromatin, characterized by the presence of RNA-mediated interference (RNAi) factors, deacetylated histones, trimethylated histone H3 Lys 9 and heterochromatin protein 1 (HP1) proteins. Although telomeric heterochromatin regulates chromosome end-processing events in telomerase-deficient settings[13–15], the function of telomeric heterochromatin in wild-type (wt) telomerase-positive cells has remained largely mysterious. Heterochromatin also surrounds centromeres and assists in the loading of specialized kinetochore proteins[16–18]. Intriguingly, although centromeres cluster beneath the SPB during mitotic interphase, they move away from the SPB during the bouquet stage, switching position with telomeres. At the same time, centromeres load meiosis-specific cohesins that ensure monopolar orientation at MI, allowing reductional segregation[19,20].

Here we demonstrate that centromeres are particularly prone to disassembly during meiotic prophase, a time not only of centromeric cohesin reorganization but also marked genome-wide chromatin remodelling. Remarkably, we find that the telomere bouquet has an unforeseen function in creating a specialized subnuclear microenvironment conducive to centromere assembly. Reassembly of compromised centromeres requires pericentromeric heterochromatin formation, which is facilitated by proximity to the bouquet. Hence, the heterochromatic nature of telomeres may have evolved to ensure centromere identity and meiotic chromosome segregation.

RESULTS

Lagging chromosomes in absence of bouquet

The SPB-controlling function of the bouquet is not fully penetrant, as deletion of the gene encoding Bqt1 leads to spindle dysfunction in only ~50% of meiocytes despite the complete absence of the bouquet in this setting[12,21]. Thus, bouquet-deficient cells harbouring functional meiotic spindles (defined as bipolar spindles of wt dynamics that segregate chromatin to opposite poles of the meiocyte, see Supplementary Fig. 1) provide a useful tool

for analysis of further defects conferred by bouquet abolition. Live imaging of these meiocytes reveals a substantial level of lagging chromosomes that remain unsegregated after spindle elongation (Fig. 1 and Supplementary Fig. 1 and Supplementary Videos 1 and 2). These lagging chromosomes originate from the same chromatin mass as properly segregating chromosomes and are not the result of nuclear fracture[22], as evident from analysis of chromatin along with nuclear membrane markers (Fig. 1 and Supplementary Fig. 1 and Supplementary Videos 3 and 4). Similar defects are observed in another bouquet-deficient genetic background in which bouquet formation is eliminated by removing Rap1 (Fig. 1 and Supplementary Fig. 1).

To determine whether the chromatin masses exhibiting failed spindle attachment harbour centromeric DNA and are not simply chromosome fragments, we used strains in which the outer repeat region of centromere I is visualized by an inserted TetO array bound to RFP-tagged Tet repressor (hereafter referred to as *cenI–TetO/R*)[23] or a LacO/LacI–GFP array at the nearby *lys1* locus (*cenI–lacO/I*); we also visualized the central core region of centromere II by an inserted TetO/R array[23] (*cenII–TetO/R*). Centromere I and II are found in the unsegregated *bqt1Δ* chromosomes in similar proportions (~12% of each fail to segregate). As chromosome III remains unsegregated in ~12% of *bqt1Δ* meiocytes, the sum of the percentages of the three individual chromosomes' segregation failure equals the percentage observed via pan-chromatin visualization (Fig. 1d,e). Hence, in the absence of the bouquet, whole centromere-containing chromatids fail to attach to the spindle.

Failed centromere assembly without bouquet

The inability of bouquet-defective chromosomes to attach to spindles suggests a defect in centromere and/or kinetochore function. We therefore monitored a battery of centromere and kinetochore components, ranging from those comprising the outer kinetochore complex, which confers direct spindle microtubule attachment, to the centromeric histone H3 variant (Cnp1, orthologue of mammalian CENP-A) on which the kinetochore complex is assembled[24–27]. The outer kinetochore complex was visualized by live analysis of meiotic cells harbouring an endogenously tagged functional allele of Dad1, a component of the DASH complex, which interacts directly with microtubules. In a wt background, Dad1 remains associated with the centromere throughout meiosis[28–30] (Supplementary Fig. 2). In contrast, the unsegregated chromosomes seen in *bqt1Δ* or *rap1Δ* meiocytes with functional spindles show defective localization of Dad1–GFP signal (Supplementary Fig. 2); in about half of the *bqt1Δ* meiocytes harbouring unsegregated chromosomes, those unsegregated chromosomes lack detectable Dad1. In other cases (~30%), the unsegregated chromosomes exhibit an unstable Dad1–GFP signal. Hence, the centromeric localization of Dad1 is erratic in the absence of the bouquet. Similar behaviour was observed for Nnf1, a component of the Mis12 outer kinetochore complex (Supplementary Fig. 3).

The absence of outer kinetochore components such as Dad1 and Nnf1 from a subset of centromeres could stem from defects in the platform for recruitment formed by the inner kinetochore. To investigate the assembly of this platform, we assessed localization of Cnp1 using ectopically expressed Cnp1–GFP under the control of the endogenous $cnp1^{+}$ promoter. Intriguingly, mild overexpression of Cnp1 confers a reduced penetrance of *bqt1Δ* centromere

attachment failure although the nature of the defects remains unchanged; unsegregated chromosomes are observed in 23% of *bqt1Δ cnp1–GFP* cells with functional spindles. Nearly half of those unsegregated chromosomes lack detectable Cnp1–GFP signal (Fig. 2a,b,e and Supplementary Videos 5 and 6), although 20% show an unstable Cnp1–GFP signal. Note that although we scored meiotic cells with functional spindles to avoid any ambiguity, kinetochore failure also occurs in *bqt1Δ* meiocytes with spindle defects (Supplementary Fig. 4). Hence, bouquet disruption confers reduced recruitment of both inner and outer kinetochore components.

To examine localization of additional factors at the base of the kinetochore, we assessed the *cenI–TetO/R* localization of endogenously tagged and functional Mis6, an essential Cnp1-loading factor[24] that remains on the centromere throughout meiosis in a wt setting[28]. The *cenI–TetO/R* signal remains unsegregated in 12.3% of *bqt1Δ* meiocytes, in line with the representation of one of the three fission yeast centromeres by *cenI–TetO/R*, and *cenI–TetO/R* fails to associate with visible Mis6–GFP in 88% of those cases (Supplementary Fig. 2d,f). Hence, the centromeres that fail to segregate in a bouquet-deficient setting tend to be devoid of detectable Mis6.

Precariousness of meiotic centromere

Our observation that meiotic centromeres often fail to assemble in the absence of the bouquet suggests that their maintenance is precarious during meiosis, or that they are actively dismantled during meiosis and re-established in a process promoted by the bouquet. Centromeric Cnp1 loading and consequent kinetochore assembly can be influenced by the presence of pericentromeric heterochromatin containing histone H3 Lys 9 trimethylation and HP1 protein[18,31,32]. To explore whether the centromere assembly defects in bouquet-deficient meiosis are accompanied by a deficiency of heterochromatin on the adjacent pericentromeres, we monitored the localization of Swi6, a fission yeast HP1 orthologue. Swi6–GFP localizes to multiple foci comprising both centromeres and telomeres in meiosis as well as mitosis[33]. As seen in cells harbouring Mis6–GFP, *cenI–TetO/R* signals remain unsegregated following meiosis in 11.5% of *bqt1Δ swi6–GFP* meiocytes exhibiting functional spindles; 83% of unsegregated *cenI–TetO/R* signals lack an associated Swi6–GFP signal (Fig. 2c,d,f and Supplementary Videos 7 and 8). Similar results were obtained using *cenII–TetO/R* (Fig. 2g). Hence, the kinetochore assembly defects seen in *bqt1Δ* meiosis are associated with, and perhaps caused by, a pericentromeric heterochromatin deficiency.

In mitotically growing cells, the establishment of new kinetochores on naive DNA sequences requires that the pericentromere be heterochromatic; in contrast, maintenance of pre-existing centromeres is independent of pericentromeric heterochromatin during mitotic growth[18]. Indeed, although mutations in *clr4*$^{+}$ (the histone H3 methyltransferase) or *dcr1*$^{+}$ (the endoribonuclease that processes double-stranded RNA into short interfering RNAs that promote heterochromatin assembly) are known to cause reduced mitotic centromere activity evinced by lagging chromosomes and minichromosome loss[34,35], the penetrance of such defects, especially chromosomes that remain unsegregated at the end of anaphase, is so low that previous studies had to employ cold treatment or microtubule-depolymerizing agents to see defects in *clr4Δ* or *dcr1Δ* backgrounds[34]. Against this backdrop, the frequency of mitotic

chromosome segregation defects (2.2% of *clr4Δ* cells) pales in comparison with the frequency of similar defects in meiosis (38.1% of *clr4Δ* meiocytes, Fig. 3a,b). A subset of these defects can be attributed to the previously reported MII segregation errors caused by loss of pericentric cohesion in the absence of Clr4 (ref. 36; Fig. 3b, green fraction). However, 40% of the defects occur in MI and cannot be linked with pericentric cohesion (Fig. 3d); moreover, a substantial fraction (33%) of chromosomes failing to attach to the spindle in *clr4Δ* meiocytes are devoid of any detectable Cnp1 (Fig. 3b,e), a deficit that cannot be explained by reduced pericentric cohesion. Similar results were obtained for mitotic versus meiotic cells lacking Dcr1 (Fig. 3a). Hence, chromosome–spindle attachment is more reliant on Clr4 and Dcr1 in meiosis than in mitosis, suggesting that meiotic centromeres are indeed prone to disassembly and need to be rebuilt.

If defective heterochromatin causes the centromere assembly defects in bouquet-deficient meiosis, mutations in heterochromatin assembly and bouquet formation pathways should be epistatic with respect to centromere assembly. Indeed, meiocytes lacking both Bqt1 and Clr4 show similar cumulative frequencies of such defects to those seen in *clr4Δ* or *bqt1Δ* single mutants (Fig. 3c and Supplementary Videos 9 and 10); likewise, *dcr1Δ bqt1Δ* and *dcr1Δ* single mutants confer similar levels of meiotic mis-segregation (Supplementary Fig. 5). However, the profiles of failed attachment differ among these backgrounds owing to two phenomena, one being the *clr4Δ* pericentric cohesion defect described above, which confers MII missegregants that harbour robust Cnp1 signals (Fig. 3d and Supplementary Fig. 5). The other phenomenon is the reduced homologue pairing and recombination conferred by *bqt1Δ* deletion but not *clr4Δ* deletion. Reduced levels of recombination render more likely the possibility that poorly assembled *bqt1Δ* centromeres are detached from properly assembled homologous centromeres and therefore discernible at MI; in contrast, poorly assembled *clr4Δ* centromeres are likely to remain indistinguishable owing to homologue pairing (Fig. 3d). Nonetheless, clear examples of unattached MI chromosomes (Fig. 3e,f and Supplementary Videos 9 and 10), often lacking Cnp1 signal (Fig. 3e and Supplementary Video 9), are seen in *clr4Δ* meiocytes, and the cumulative occurrence of unattached centromeres lacking Cnp1 in *clr4Δ*, *bqt1Δ* and *clr4Δ bqt1Δ* meiocytes is similar (Fig. 3c). These epistatic relationships suggest that the centromere attachment defects of bouquet-deficient cells stem at least in part from defects in the Clr4-and RNAi-mediated heterochromatin assembly pathway.

As bouquet-deficient strains sustain defects in prophase chromosome movement, homologue pairing and recombination, we considered the possibility that these defects underlie the incomplete centromere assembly. To address this, we examined kinetochore function in bouquet-proficient strains lacking the dynein heavy chain Dhc1, which is required for horsetail nuclear movements and wt levels of meiotic recombination[2,3,37–39]. Unsegregated chromosomes are seen in 17.5% of *dhc1Δ* meiocytes, in line with the merotelic attachments expected to stem from reduced recombination. However, robust Cnp1–GFP signals are observed on all unsegregated chromosomes in *dhc1Δ* meiocytes (Fig. 4). Hence, centromere assembly defects do not result from reduced meiotic nuclear movement or recombination, but rather are specific for meiotic cells lacking the bouquet. In contrast to bouquet-proficient *dhc1Δ* meiocytes, 25% of *dhc1Δ bqt1Δ* meiocytes sustain unsegregated chromosomes devoid of Cnp1 signal, indicating that *bqt1Δ* centromere assembly defects are not suppressed

by *dhc1* deletion, and are therefore a result neither of SPB movement nor of movement-induced separation of individual chromosomes from the main nuclear mass (Fig. 4).

Centromere–telomere co-localization

There are several means by which telomeres could affect meiotic centromere assembly. Conceivably, the influence of the bouquet on centromere function could be mediated by a diffusible factor emanating from the bouquet, or by the propagation of a factor along the chromosome from the bouquet to the centromere. Alternatively, contact with the telomere may confer its effects on the centromere. As the centromeres cluster at the SPB throughout mitotic interphase, a transient telomere–centromere contact could exist as an intermediate stage in the switch between centromere–SPB and telomere–SPB associations; this stage could provide an opportunity for telomeres to affect centromeres through proximity. Indeed, co-localization of centromeres and telomeres was observed in cells arrested in a state in which they have undergone sexual differentiation and extruded a conjugation tube but failed to conjugate[40]. To determine whether such telomere–centromere contact is part of meiotic progression in a wt setting, we imaged telomeres and centromeres (via endogenously tagged and functional Taz1 and Mis6, respectively) every 18 s through early prophase. Of 6 films taken at these closely spaced time points, all show extended periods of centromere–telomere co-localization as the bouquet forms (example shown in Fig. 5a and Supplementary Video 11). We find not only that telomeres and centromeres co-localize in the period between centromere–SPB and telomere–SPB clustering, but also that the process occurs in a stepwise fashion. Following the arrival of a subset of telomeres at the SPB, a fraction of the centromere signal can be seen to separate from the SPB; subsequently, additional telomeres arrive and remaining centromeres gradually leave. This contact between telomeres and centromeres renders viable the possibility that telomeres directly modify centromeres or create a local microenvironment conducive to centromere assembly.

Microenvironment promotes centromere assembly

To explore the idea of such a microenvironment, we used a strain in which the lethality resulting from deletion of *trt1*$^{+}$ (which encodes the catalytic subunit of telomerase) has been overcome by circularization of each of the three *Schizosaccharomyces pombe* chromosomes; these circular chromosomes are devoid of telomeres[41–43]. Although such strains are viable during mitotic growth, they fail to form the bouquet and sustain meiotic spindle formation defects reminiscent of those seen in bouquet-deficient strains. However, insertion of an interstitial telomere repeat stretch on one (Chr III) of the three circular chromosomes (producing the strain hereafter referred to as circular + internal telo) results in localization of the ectopic telomere stretch to the SPB during meiotic prophase and rescues meiotic spindle formation[21]. Nonetheless, chromosomes can still be seen failing to attach to the spindle in ~18% of circular + internal telo meiocytes, and these unattached chromosomes lack Cnp1–GFP signal (Supplementary Fig. 6). To address the influence of telomere–centromere proximity, we investigated whether centromere attachment defects are confined to those chromosomes lacking the internal telomere repeat stretch, which can be readily identified via its associated Taz1–YFP signal. Of 80 such circular + internal telo meiocytes, 12 sustained chromosomes that failed to attach to the meiotic spindle. Strikingly, however, in none of those 12 meiocytes was Chr III, the chromosome harbouring the internal telomere,

the one that failed to attach to the spindle (Fig. 5b,d and Supplementary Video 12). Importantly, we find that Chr III is not inherently protected from spindle attachment defects, as Chr III shows centromere assembly defects and attachment failure as often as other chromosomes in *bqt1Δ* strains with linear chromosomes (Fig. 1e, Supplementary Fig. 7); hence, protection in the circular + internal telo background is specifically afforded by the internal telomere stretch. In a complementary experiment, we monitored the segregation of Chr I in the circular + internal telo background via *cenI–lacO/I*. Of 76 such meiocytes filmed, 11 sustained an unattached chromosome, 6 of those harbouring *cenI–lacO/I* (Fig. 5c,e). Hence, the internal telomere repeat tract confers robust function to the centromere borne by the same chromosome, but not the centromeres of other chromosomes, which often localize to regions of the nucleus far from the internal telomere tract (Fig. 5b–e).

The ability of the internal telomere to safeguard centromere assembly in *cis* could be explained either by a proximity effect in which the connectivity between the telomere and centromere guarantees that the two will be in the same vicinity for some threshold period of time, or by a propagation effect in which a factor moves along the chromosome from telomere to centromere. To distinguish between these possibilities, we used strains harbouring *cenI–lacO/I* in combination with a fusion between Bqt1 and the GFP-binding protein[44] (GBP) in a circular + internal telo background. This construct tethers *cenI* to the SPB and therefore to the vicinity of the internal telomere on Chr III. In this setting, the centromere of ChrI is completely rescued from non-attachment, while Chr II often shows non-attachment events (Fig. 6 and Supplementary Video 13). Crucially, this rescue depends on the presence of the internal telomere at the SPB, as the Bqt1-GBP-*cenI–lacO/I* linkage fails to afford proper centromere I assembly when the internal telomere is absent (Fig. 6). Hence, centromere assembly is promoted by proximity to the SPB-associated telomere.

Such proximity dependence predicts a linear correlation between the number of telomeres detached from the bouquet in a given meiocyte and the probability of that meiocyte suffering unattached chromosomes. Indeed, examination of 5 strains with different numbers of telomeres participating in the bouquet reveals a clear linear correlation between these two variables (Fig. 7). Hence, the bouquet creates a local environment conducive to centromere assembly.

The bouquet microenvironment has two conspicuous properties, the presence of telomeres and the presence of the SPB, either or both of which could confer the ability of the bouquet to promote local centromere assembly. To consider the SPB localization facet in isolation, we exploited the *dhc1Δ bqt1Δ* meiocytes described above along with the observation that a subset of centromeres remain associated with the SPB throughout meiotic prophase in this background[22]. Notably, the appearance of unsegregated chromatin masses lacking Cnp1–GFP is not suppressed by this greatly enhanced level of centromere–SPB association (Fig. 4). Moreover, we find examples of cells in which the precise centromere that remains associated with the SPB fails to segregate at MI (Fig. 8). Hence, the association of centromeres with SPBs that lack associated telomeres does not promote meiotic centromere assembly.

DISCUSSION

The clustering of telomeres within the bouquet creates a region in which telomere-specific factors are concentrated; likewise, factors related to the heterochromatic state of the telomeres, such as Lys-9-methylated histone H3, Swi6 and non-coding RNA, will also be concentrated in this region[45,46]. Notably, many of the factors in this microenvironment play key roles in centromere assembly, lending a plausible explanation for the observation that localization of centromeres to this microenvironment enhances the probability of correct assembly. This principle is particularly germane as meiotic centromeres are far more susceptible to disruption by heterochromatin defects than mitotic centromeres (Fig. 3a,b); moreover, the pericentric heterochromatin is also susceptible to disruption during meiosis (Fig. 2d,f,g). Indeed, our data suggest that a subset of centromeres need to be reassembled during meiosis, thus mirroring the requirement of pericentromeric heterochromatin for mitotic centromere establishment[18] (as opposed to the lack of a requirement of pericentric heterochromatin for mitotic centromere maintenance). The enhanced susceptibility of meiotic centromeres to disruption may stem from sequestration of silencing factors to the telomeric microenvironment as the organism strives to prevent the spread of telomere-proximal transposons in the germ line, or may reflect the widespread chromatin remodelling that occurs during meiosis and promotes the expression of meiosis-specific genes. Disruption of meiotic centromeres may also result from centromeric restructuring associated with the switch from competency for equational mitotic chromosome segregation to reductional MI segregation; the regulated loss of outer kinetochore proteins from centromeres during meiotic prophase[47] could conceivably promote disassembly of nearby chromatin. Enhanced susceptibility to centromeric disruption may be shared by other cell types or developmental stages in which substantial chromatin remodelling occurs.

The precise stage during which telomeres modify centromere assembly remains to be determined. As telomere recruitment to the SPB at prophase onset is accompanied by gradual centromere release, the period of bouquet formation would provide an ideal setting for telomere–centromere proximity. When several telomeres are present in bouquet-proficient cells, it may be virtually guaranteed that at least one telomere is available to modify each centromere before it is released from the SPB; in contrast, when few telomeres are present, as in the circular + internal telo scenario, some centromeres may move away from the SPB before any telomere arrives.

The impressive conservation of telomere components and principles of function raise the possibility that the meiotic roles of telomeres are also conserved. Indeed, a previous report showed chromosome attachment defects in fourth-generation telomerase-minus mouse oocytes[48], suggesting that kinetochore dysfunction may occur in oocytes following the loss of functional telomeres. Hence, the role of telomeres in promoting centromere organization may be conserved. We find that 2–4% of all individual centromeres become dysfunctional in bouquet-deficient fission yeast meiocytes. As the human germ cell carries 92 centromeres, such a percentage would be enough to make several centromeres dysfunctional in every human meiosis. Thus, this unanticipated role of the telomere bouquet may be important for understanding human meiotic chromosome non-disjunction, which leads to miscarriages and genetic diseases such as Down’s syndrome.

METHODS

Methods and any associated references are available in the online version of the paper.

METHODS

Yeast strains and media.

Details of strains used are presented in Supplementary Table 1. All media were as described[49]. Gene deletions and tag insertions were created by the one-step gene replacement method[50]. The *kanMX6* cassette was, as the need arose, switched to *hygMX6* (*HphMX6*; refs 51,52), *his3*+ (*his3*+*MX6*) or *leu1*+(*kanMX6::leu1*+; ref. 12). For replacements with *ura4*, fragments were amplified from pKS-ura4 (ref. 53). Multiply mutated genotypes were produced by mating combinations of strains. The synthetic telomere insert strains were constructed as described previously[21].

For most strains harbouring tagged proteins, both mitotic and meiotic cell cycles progress normally. However, strains harbouring *pnmt1:GFP–atb2* show an elevated prevalence of meiotic lagging chromosomes in an otherwise wt background (2.5% in wt versus 10% in *pnmt1:GFP–atb2*).

Strains harbouring *lys1::cnp1–GFP* produce smaller colonies than wt strains in mitotic culture but behave normally in meiosis. When *bqt1* is deleted, the strains with this mild overexpression of Cnp1 show a lower incidence of chromosome–spindle non-attachment (23% compared with ~30% in cells expressing wt levels of Cnp1). Hence, perhaps unsurprisingly, mild Cnp1 overexpression partially suppresses the *bqt1Δ* centromere assembly defect.

clr4Δ strains exhibit a mating-type switching deficiency in homothallic strains[54,55]. For this reason we included *h+*× *h−* matings of *clr4Δ* and *clr4Δ bqt1Δ* strains in addition to the h^{90} strains. No significant difference was observed between h^{90} or *h+/−* matings.

For experiments examining zygotic meiosis, cells were grown at 32 °C in YES media, washed and meiotically induced by incubating h^{90} or a mixture of *h−* and *h+* cells on ME plates at 30 °C for approximately 7 h before starting analysis by live microscopy (described below). For meiotic synchronization of azygotic cells, cultures were grown at 32 °C in YES to a density of 1×10^7 cells ml^{-1}, collected, washed and re-suspended in EMM (+N) and grown at 32 °C to a density of 1×10^7 cells ml^{-1}. Cells were collected, washed three times and re-suspended in EMM (−N) +0.5% glucose to a final density of 0.5×10^7 cells ml^{-1}, and incubated at 30 °C with vigorous shaking for meiotic induction. Zygotes (referred to as meiocytes or meiotic cells throughout the manuscript) were filmed at intervals from 4 to 7 h post-meiotic induction.

Live microscopy.

Live analysis was carried out by adhering cells to 35 mm glass culture dishes (MatTek) precoated with 0.2 mg ml^{-1} soybean lectin (Calbiochem) and immersing them in EMM-N with required supplements (+0.2 mM thiamine for Pnmt1–GFP–Atb2). Cells were imaged

on a DeltaVision Spectris (Applied Precision) comprising an Olympus IX71 wide-field inverted fluorescence microscope, an Olympus UPlanSApo 1003, NA 1.35, oil immersion objective, and a Photometrics CCD CH350 camera cooled to −35 °C (Roper Scientific), or a DeltaVision Elite (Applied Precision) comprising an Olympus IX71 wide-field inverted fluorescence microscope, an Olympus PLAPON100xO, NA 1.42, oil immersion objective, and a Photometrics CoolSnap HQ2 camera, or a DeltaVision OMX (Applied Precision) comprising an OMX optical microscope (version 4), an Olympus PLAPON60xO, NA 1.42, oil immersion objective, and a sCMOS camera. Culture dishes were incubated at 27 °C in the integrated environmental chamber. Images were captured and analysed using softWoRx (Applied Precision), deconvolved and combined into maximal intensity projections. For long-term time course experiments, 9.1 μm of *Z*-axis imaging was acquired with optical axis integration. Coverage of the entire cell required a sweep lasting approximately 3 s, and this was repeated every 10 min for approximately 5 h. For the centromere array experiments we shifted between filter sets on each *Z* section, before moving on to the next *Z* section. This way, we avoided the potential problem of centromeres moving during the 3 s required to sweep the cell. Further experiments showed that owing to our scoring system (see below), in which only those centromeres that are well separated in space are scored, there was no significant difference between switching filters between each *Z* section or between each sweep.

Analysis of kinetochore foci.

To assess kinetochore function, we scored only those cells exhibiting proper bipolar spindle formation as evinced by the movement of DNA masses to opposite poles along clearly visible stable spindles in MI and/or MII, or in strains lacking fluorescently tagged tubulin, along the trajectory connecting SPB signals that move apart symmetrically to opposite poles. The validity of this latter approach was assessed by scoring meiocytes harbouring the same kinetochore markers with and without fluorescent tubulin. Kinetochore signals obtained from cells with fluorescent tubulin are fainter owing to photobleaching; nevertheless, the effects of bouquet deficiency on kinetochore assembly follow the same pattern in meiocytes with or without tagged tubulin (data not shown). The symmetrical pulling of DNA masses to opposite poles also serves as a marker for spindle formation when no tubulin or SPB markers are present in ‘circular’ strains (in which all markers are exhausted); note that proper spindle formation is successfully conferred by either the presence of an internal telomere stretch (in the circular + internal telo setting), or a tethered centromere, at the prophase SPB (refs 7,22).

To assess whether a kinetochore focus co-localizes with a chromatin signal, we quantified imaging data as follows. Images were deconvolved using the DeltaVision Spectris (Applied Precision) software; the resulting images were then analysed using Volocity software. Background signal values were assigned by averaging the signal/volume associated with two spherical areas in the cytoplasm and subtracted in all further analyses. The background-subtracted intensities of all kinetochore signals co-localizing with DNA masses were then summed. A signal whose intensity was below 1/12 of the total kinetochore signal for a given MI/MII cell was considered undetectable, as the meiotic cell harbours 12 centromeres from late prophase onwards. A chromosome was scored as lacking a kinetochore signal if

kinetochore signal associated with that chromosome remained undetectable for at least 3 consecutive frames. Kinetochore signals were scored as stable if they were detectable on chromatin in at least 5 of the first 7 frames after anaphase I or II (frames are taken every 10 min). If the signal could be detected in less than 5 of the first 7 frames after anaphase I or II, it was deemed unstable.

Statistical analysis was performed using Fisher's exact test (http://www.langsrud.com/fisher.htm). Fisher's test is used for samples with a low *n*, accumulated over time. Thus, we calculated the *P* value for the entire set of cells we filmed for every genotype. If a sample size of 150 cells per genotype failed to yield significance, differences were deemed insignificant. Note that in all of our experiments, only a subset of the filmed cells were taken for analysis (because of failure of spindle formation in many cases); thus, the 150 sample size represents at least twice the number of meiocytes filmed. For kinetochore foci, the fraction of cells lacking stable kinetochore signals was compared among the different genotypes. Therefore, the statistical significance scores express that of the difference in kinetochore activity between these genotypes.

Supplementary Material

Refer to Web version on PubMed Central for supplementary material.

ACKNOWLEDGEMENTS

We thank our current and former laboratory members for discussions and advice, and R. Allshire (Wellcome Trust, University of Edinburgh, UK), M. Sato (University of Tokyo, Japan), T. Toda (Cancer Research UK, UK) and Y. Watanabe (University of Tokyo, Japan) for strains and reagents. We thank M. Lichten, S. Grewal and their laboratory members for discussion and help with reagents and equipment during our recent move. This work was supported by the National Institutes of Health, Cancer Research UK, the European Research Council, and a Marie Curie fellowship to M.K.

References

1. Klutstein M & Cooper JP The Chromosomal Courtship Dance-homolog pairing in early meiosis. Curr. Opin. Cell Biol 26, 123–131 (2014). [PubMed: 24529254]
2. Yoshida M et al. Microtubule-organizing center formation at telomeres induces meiotic telomere clustering. J. Cell Biol 200, 385–395 (2013). [PubMed: 23401002]
3. Ding DQ, Yamamoto A, Haraguchi T & Hiraoka Y Dynamics of homologous chromosome pairing during meiotic prophase in fission yeast. Dev. Cell 6, 329–341 (2004). [PubMed: 15030757]
4. Cooper JP, Watanabe Y & Nurse P Fission yeast Taz1 protein is required for meiotic telomere clustering and recombination. Nature 392, 828–831 (1998). [PubMed: 9572143]
5. Chikashige Y et al. Meiotic proteins bqt1 and bqt2 tether telomeres to form the bouquet arrangement of chromosomes. Cell 125, 59–69 (2006). [PubMed: 16615890]
6. Ding X et al. SUN1 is required for telomere attachment to nuclear envelope and gametogenesis in mice. Dev. Cell 12, 863–872 (2007). [PubMed: 17543860]
7. Conrad MN et al. Rapid telomere movement in meiotic prophase is promoted by NDJ1, MPS3, and CSM4 and is modulated by recombination. Cell 133, 1175–1187 (2008). [PubMed: 18585352]
8. Chua PR & Roeder GS Tam1, a telomere-associated meiotic protein, functions in chromosome synapsis and crossover interference. Genes Dev. 11, 1786–1800 (1997). [PubMed: 9242487]
9. Davis L & Smith GR The meiotic bouquet promotes homolog interactions and restricts ectopic recombination in *Schizosaccharomyces pombe*. Genetics 174, 167–177 (2006). [PubMed: 16988108]

10. Nimmo ER, Pidoux AL, Perry PE & Allshire RC Defective meiosis in telomere-silencing mutants of *Schizosaccharomyces pombe*. Nature 392, 825–828 (1998). [PubMed: 9572142]
11. Niwa O, Shimanuki M & Miki F Telomere-led bouquet formation facilitates homologous chromosome pairing and restricts ectopic interaction in fission yeast meiosis. EMBO J. 19, 3831–3840 (2000). [PubMed: 10899136]
12. Tomita K & Cooper JP The telomere bouquet controls the meiotic spindle. Cell 130, 113–126 (2007). [PubMed: 17632059]
13. Jain D, Hebden AK, Nakamura TM, Miller KM & Cooper JP HAATI survivors replace canonical telomeres with blocks of generic heterochromatin. Nature 467, 223–227 (2010). [PubMed: 20829796]
14. O' Sullivan RJ et al. Rapid induction of alternative lengthening of telomeres by depletion of the histone chaperone ASF1. Nat. Struct. Mol. Biol 21, 167–174 (2014). [PubMed: 24413054]
15. Heaphy CM et al. Altered telomeres in tumors with ATRX and DAXX mutations. Science 333, 425 (2011). [PubMed: 21719641]
16. Kawashima SA et al. Shugoshin enables tension-generating attachment of kinetochores by loading Aurora to centromeres. Genes Dev. 21, 420–435 (2007). [PubMed: 17322402]
17. Bernard P et al. Requirement of heterochromatin for cohesion at centromeres. Science 294, 2539–2542 (2001). [PubMed: 11598266]
18. Folco HD, Pidoux AL, Urano T & Allshire RC Heterochromatin and RNAi are required to establish CENP-A chromatin at centromeres. Science 319, 94–97 (2008). [PubMed: 18174443]
19. Yokobayashi S & Watanabe Y The kinetochore protein Moa1 enables cohesion-mediated monopolar attachment at meiosis I. Cell 123, 803–817 (2005). [PubMed: 16325576]
20. Kitajima TS, Kawashima SA & Watanabe Y The conserved kinetochore protein shugoshin protects centromeric cohesion during meiosis. Nature 427, 510–517 (2004). [PubMed: 14730319]
21. Tomita K, Bez C, Fennell A & Cooper JP A single internal telomere tract ensures meiotic spindle formation. EMBO Rep. 14, 252–260 (2013). [PubMed: 23295325]
22. Fennell A, Fernandez-Alvarez A, Tomita K & Cooper JP Telomeres and centromeres have interchangeable roles in promoting meiotic spindle formation. J. Cell Biol 208, 415–428 (2015). [PubMed: 25688135]
23. Sakuno T, Tada K & Watanabe Y Kinetochore geometry defined by cohesion within the centromere. Nature 458, 852–858 (2009). [PubMed: 19370027]
24. Takahashi K, Chen ES & Yanagida M Requirement of Mis6 centromere connector for localizing a CENP-A-like protein in fission yeast. Science 288, 2215–2219 (2000). [PubMed: 10864871]
25. Palmer DK, O'Day K, Wener MH, Andrews BS & Margolis RLA 17-kD centromere protein (CENP-A) copurifies with nucleosome core particles and with histones. J. Cell Biol 104, 805–815 (1987). [PubMed: 3558482]
26. Vafa O & Sullivan KF Chromatin containing CENP-A and -satellite DNA is a major component of the inner kinetochore plate. Curr. Biol 7, 897–900 (1997). [PubMed: 9382804]
27. Blower MD & Karpen GH The role of *Drosophila* CID in kinetochore formation, cell-cycle progression and heterochromatin interactions. Nat. Cell Biol 3, 730–739 (2001). [PubMed: 11483958]
28. Hayashi A, Asakawa H, Haraguchi T & Hiraoka Y Reconstruction of the kinetochore during meiosis in fission yeast *Schizosaccharomyces pombe*. Mol. Biol. Cell 17, 5173–5184 (2006). [PubMed: 17035632]
29. Sanchez-Perez I et al. The DASH complex and Klp5/Klp6 kinesin coordinate bipolar chromosome attachment in fission yeast. EMBO J. 24, 2931–2943 (2005). [PubMed: 16079915]
30. Liu X, McLeod I, Anderson S, Yates JR III & He X Molecular analysis of kinetochore architecture in fission yeast. EMBO J. 24, 2919–2930 (2005). [PubMed: 16079914]
31. Smith KM, Phatale PA, Sullivan CM, Pomraning KR & Freitag M Heterochromatin is required for normal distribution of *Neurospora crassa* CenH3. Mol. Cell. Biol 31, 2528–2542 (2011). [PubMed: 21505064]

32. Nakashima H et al. Assembly of additional heterochromatin distinct from centromere-kinetochore chromatin is required for de novo formation of human artificial chromosome. J. Cell Sci 118, 5885–5898 (2005). [PubMed: 16339970]
33. Ekwall K et al. The chromodomain protein Swi6: a key component at fission yeast centromeres. Science 269, 1429–1431 (1995). [PubMed: 7660126]
34. Ekwall K et al. Mutations in the fission yeast silencing factors clr4+ and rik1+ disrupt the localisation of the chromo domain protein Swi6p and impair centromere function. J. Cell Sci 109, 2637–2648 (1996). [PubMed: 8937982]
35. Volpe T et al. RNA interference is required for normal centromere function in fission yeast. Chromosome Res. 11, 137–146 (2003). [PubMed: 12733640]
36. Kitajima TS, Yokobayashi S, Yamamoto M & Watanabe Y Distinct cohesin complexes organize meiotic chromosome domains. Science 300, 1152–1155 (2003). [PubMed: 12750522]
37. Yamamoto A, West RR, McIntosh JR & Hiraoka Y A cytoplasmic dynein heavy chain is required for oscillatory nuclear movement of meiotic prophase and efficient meiotic recombination in fission yeast. J. Cell Biol 145, 1233–1249 (1999). [PubMed: 10366596]
38. Hiraoka Y, Ding DQ, Yamamoto A, Tsutsumi C & Chikashige Y Characterization of fission yeast meiotic mutants based on live observation of meiotic prophase nuclear movement. Chromosoma 109, 103–109 (2000). [PubMed: 10855500]
39. Chikashige Y et al. Chromosomes rein back the spindle pole body during horsetail movement in fission yeast meiosis. Cell Struct. Funct 39, 93–100 (2014). [PubMed: 24954111]
40. Chikashige Y et al. Meiotic nuclear reorganization: switching the position of centromeres and telomeres in the fission yeast *Schizosaccharomyces pombe*. EMBO J. 16, 193–202 (1997). [PubMed: 9009280]
41. Naito T, Matsuura A & Ishikawa F Circular chromosome formation in a fission yeast mutant defective in two ATM homologues. Nat. Genet 20, 203–206 (1998). [PubMed: 9771717]
42. Sadaie M, Naito T & Ishikawa F Stable inheritance of telomere chromatin structure and function in the absence of telomeric repeats. Genes Dev. 17, 2271–2282 (2003). [PubMed: 12952894]
43. Nakamura TM, Cooper JP & Cech TR Two modes of survival of fission yeast without telomerase. Science 282, 493–496 (1998). [PubMed: 9774280]
44. Dodgson J et al. Spatial segregation of polarity factors into distinct cortical clusters is required for cell polarity control. Nat. Commun 4, 1834 (2013). [PubMed: 23673619]
45. Schober H, Ferreira H, Kalck V, Gehlen LR & Gasser SM Yeast telomerase and the SUN domain protein Mps3 anchor telomeres and repress subtelomeric recombination. Genes Dev. 23, 928–938 (2009). [PubMed: 19390087]
46. Taddei A et al. The functional importance of telomere clustering: global changes in gene expression result from SIR factor dispersion. Genome Res. 19, 611–625 (2009). [PubMed: 19179643]
47. Asakawa H, Hayashi A, Haraguchi T & Hiraoka Y Dissociation of the Nuf2-Ndc80 complex releases centromeres from the spindle-pole body during meiotic prophase in fission yeast. Mol. Biol. Cell 16, 2325–2338 (2005). [PubMed: 15728720]
48. Liu L, Blasco MA & Keefe DL Requirement of functional telomeres for metaphase chromosome alignments and integrity of meiotic spindles. EMBO Rep. 3, 230–234 (2002). [PubMed: 11882542]
49. Moreno S, Klar A & Nurse P Molecular genetic analysis of fission yeast *Schizosaccharomyces pombe*. Methods Enzymol. 194, 795–823 (1991). [PubMed: 2005825]
50. Bahler J et al. Heterologous modules for efficient and versatile PCR-based gene targeting in *Schizosaccharomyces pombe*. Yeast 14, 943–951 (1998). [PubMed: 9717240]
51. Hentges P, Van Driessche B, Tafforeau L, Vandenhaute J & Carr AM Three novel antibiotic marker cassettes for gene disruption and marker switching in *Schizosaccharomyces pombe*. Yeast 22, 1013–1019 (2005). [PubMed: 16200533]
52. Sato M, Dhut S & Toda T New drug-resistant cassettes for gene disruption and epitope tagging in *Schizosaccharomyces pombe*. Yeast 22, 583–591 (2005). [PubMed: 15942936]

53. Grimm C, Kohli J, Murray J & Maundrell K Genetic engineering of *Schizosaccharomyces pombe*: a system for gene disruption and replacement using the ura4 gene as a selectable marker. Mol. Gen. Genet 215, 81–86 (1988). [PubMed: 3241624]

54. Lorentz A, Ostermann K, Fleck O & Schmidt H Switching gene swi6, involved in repression of silent mating-type loci in fission yeast, encodes a homologue of chromatin-associated proteins from *Drosophila* and mammals. Gene 143, 139–143 (1994). [PubMed: 8200530]

55. Bannister AJ et al. Selective recognition of methylated lysine 9 on histone H3 by the HP1 chromo domain. Nature 410, 120–124 (2001). [PubMed: 11242054]

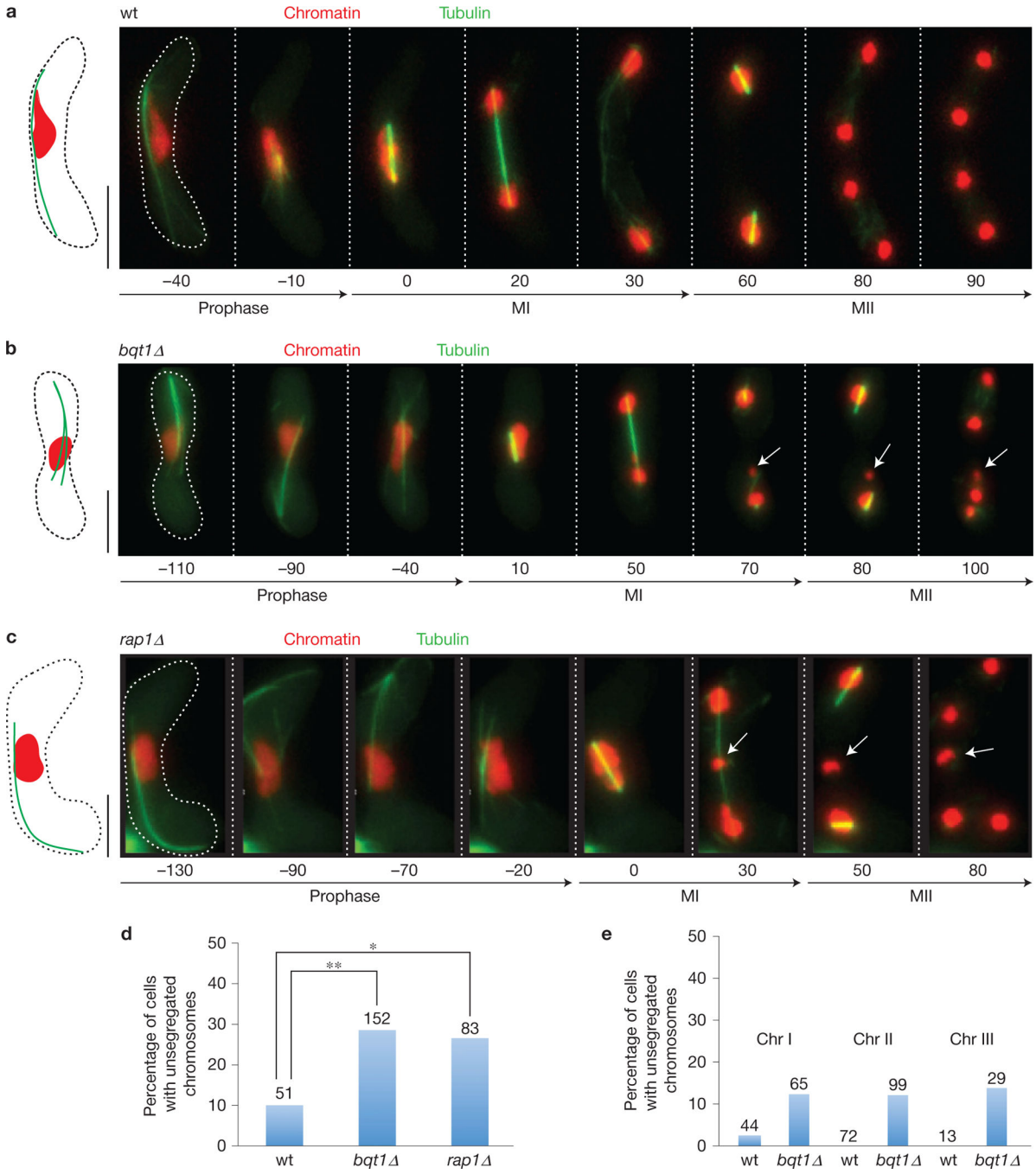

Figure 1.

Bouquet-deficient meiocytes show failure of chromosome attachment to correctly formed spindles. (**a–c**) Series of frames from films of cells undergoing meiosis. Tubulin and histone H3 are observed via ectopically expressed GFP–Atb2 (green) and endogenous mRFP tagging of one of the two alleles encoding Hht1 (red), respectively. Numbers below frames represent minutes before or after MI. Scale bars represent 5 μm. (**a**) wt meiosis. All chromosomes attach properly to bipolar spindles at MI and MII. See also Supplementary Video 1. (**b**) *bqt1Δ* meiosis. The spindle forms correctly but some chromosomes (arrows)

fail to attach to those spindles and remain unsegregated. See also Supplementary Video 2. (**c**) *rap1Δ* meiosis. Failed spindle attachment is seen for some chromosomes (arrows) as in *bqt1Δ* meiosis. (**d**) Quantification of the frequency of non-attachment events as observed via tagged histone H3 (expressed as percentage of cells with a chromosome remaining in the middle after metaphase). Number of cells filmed is indicated above each lane. Asterisk indicates significant differences from wt calculated using Fisher's exact test (wt–*bqt1Δ P* =0.007, wt–*rap1 P* = 0.02, see Methods for details). (**e**) Frequency of non-attachment events of individual chromosomes expressed as the percentage of cells with a centromere or sub-telomeric region remaining unsegregated after anaphase. Chr I non-attachment was scored via the *cenI–TetO/R* system (see text). Chr II non-attachment was scored via the *cenII–TetO/R* system (see text). Chr. III non-attachment was scored via Reb1–GFP (see text). The sum of percentages for each individual chromosome matches the overall rate shown in **d**, indicating that whole chromosomes (rather than fragments) fail to segregate. Number of cells filmed is indicated above each bar.

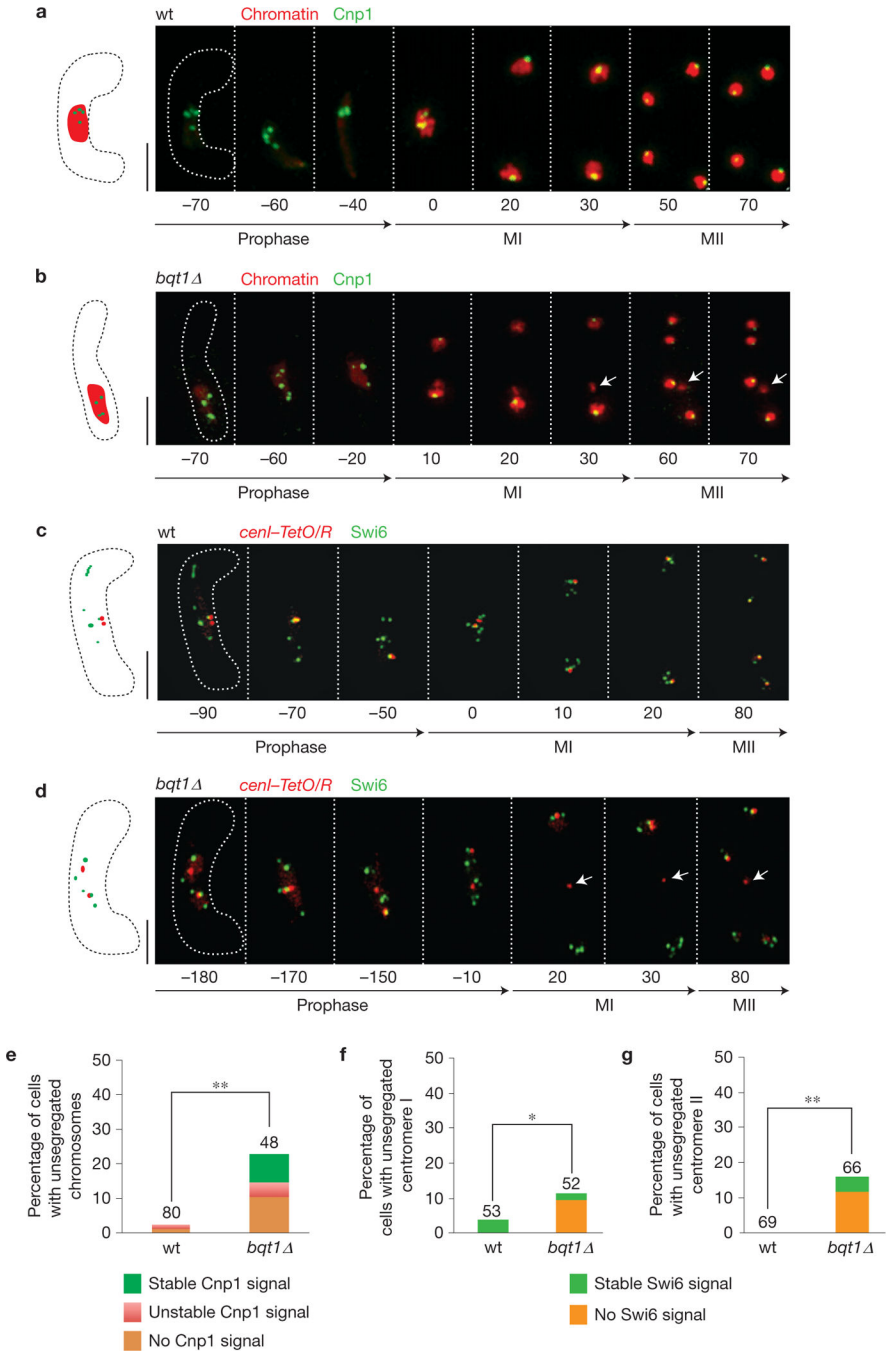

Figure 2.

Bouquet-deficient meiocytes fail to properly assemble kinetochores. (**a,b**) Series of frames from films of cells undergoing meiosis. Cnp1 and chromatin are observed via ectopically expressed Cnp1–GFP (see text) and Hht1–mRFP (as in Fig. 1), respectively. Labels as in Fig. 1. (**a**) wt meiosis. Cnp1–GFP appears at all chromatin masses at MI and MII. (**b**) *bqt1Δ* meiosis. Some chromosomes (arrows) fail to recruit Cnp1 and remain unsegregated. (**c,d**) Series of frames from films of cells undergoing meiosis. Endogenously tagged functional Swi6–GFP is observed along with *cenI–TetO/R*. (**c**) wt meiosis. Swi6–GFP is correctly

recruited to centromere I. (**d**) *bqt1Δ* meiosis. In some cases centromere I fails to recruit Swi6 and remains unsegregated (arrows). Scale bars in **a–d** represent 5 μm. (**e**) Quantification of Cnp1 localization to unsegregated chromosomes. The superimposed colour code specifies the pattern of Cnp1–GFP signal in each genetic background. See Methods for definitions of stable and unstable. Number of cells filmed is indicated above each lane. Asterisks indicate significant difference from wt calculated using Fisher's exact test (wt–*bqt1Δ* P =0.0003). (**f**) Quantification of Swi6 localization on centromere I. Labels as in e (wt–*bqt1Δ* P =0.02). (**g**) Quantification of Swi6 localization on centromere II (visualized via *cenII–TetO/R*). Labels as in e (wt–*bqt1Δ* P =0.002, see Methods for details).

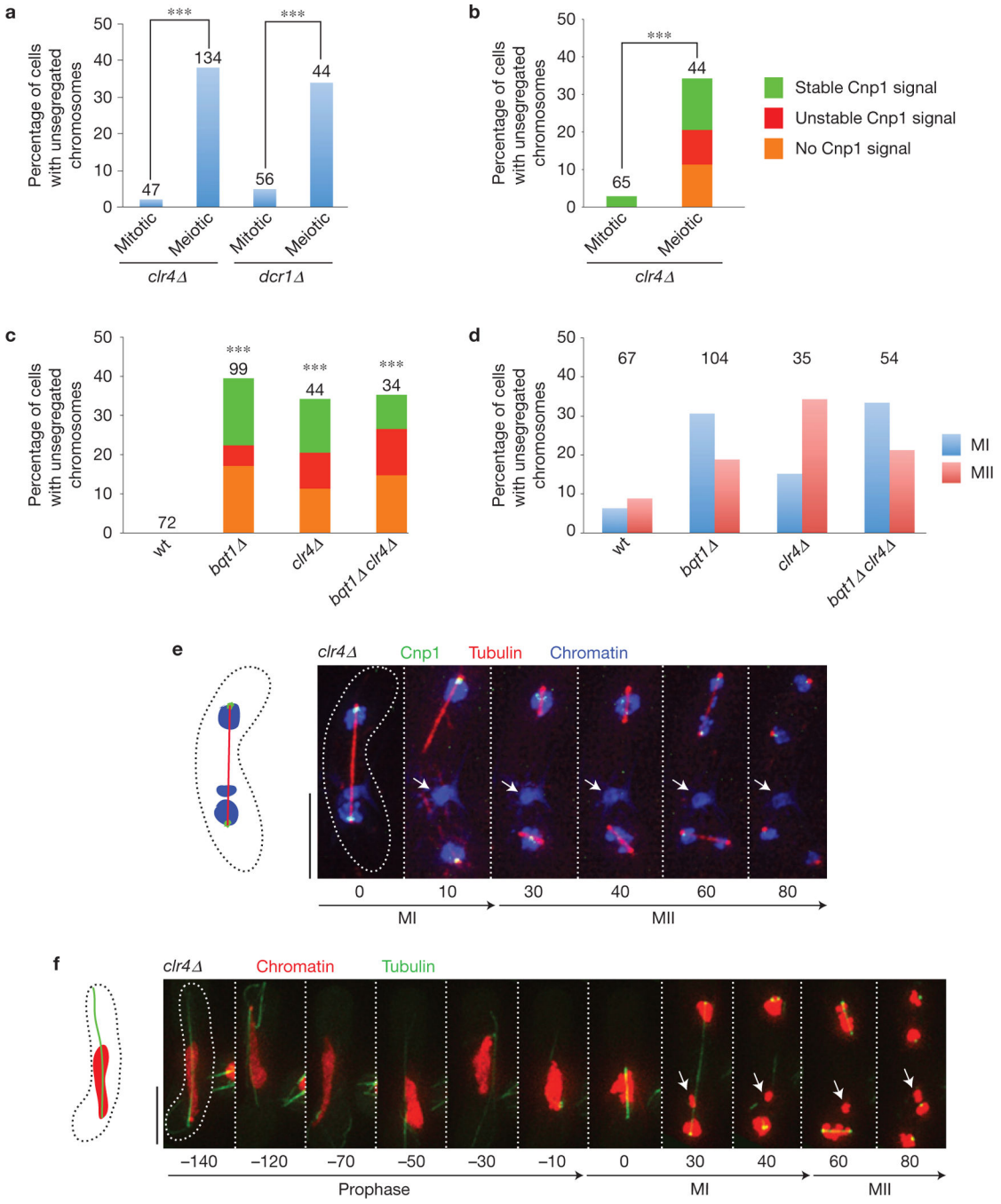

Figure 3.

Meiocytes deficient in pericentromeric heterochromatin formation show centromere assembly defects. (**a**) Comparison of requirement for heterochromatin assembly factors for centromere function in mitosis versus meiosis. Frequencies of non-attachment events observed via GFP–Atb2 Hht1–mRFP (as in Fig. 1) are shown (*clr4Δ* mitotic–*clr4Δ* meiotic $P = 3\times10^{-7}$; *dcr1Δ* mitotic–*dcr1Δ* meiotic $P = 0.0003$). Number of cells filmed is indicated above each bar. (**b**) Comparison of requirement of heterochromatin assembly factors for Cnp1 loading in mitosis versus meiosis. The superimposed colour code specifies the pattern

of Cnp1–GFP signal on those centromeres (mitotic–meiotic P =0.00005). Number of cells filmed is indicated above each bar. See Methods for designation of stable and unstable signals. (**c**) Genetic epistasis analysis of Cnp1 localization on centromeres. The superimposed colour code specifies the pattern of Cnp1–GFP signal as in **b**. Number of cells filmed is indicated above each bar. Asterisks indicate that all mutant backgrounds differ significantly from wt; no significant differences are observed among the various mutant genotypes (wt–*bqt1Δ* $P = 10^{-5}$, wt–*clr4Δ* $P = 10^{-4}$, wt–*clr4Δ bqt1Δ* P =0.0002). (**d**) Comparison of segregation defects in MI (blue) versus MII (red) in the indicated backgrounds. Frequencies of non-attachment events observed via GFP–Atb2 Hht1–mRFP (as in Fig. 1) are shown. Number of cells filmed is indicated above each bar. *bqt1Δ* and *bqt1Δ clr4Δ* meiocytes exhibit more defects in MI in contrast to *clr4Δ* meiocytes show more defects in MII (see text for explanation). (**e**) Series of frames from films of cells undergoing meiosis. Cnp1, tubulin and chromatin are observed via ectopically expressed Cnp1–GFP, Atb2–mCherry and Hht1–CFP, respectively. Labels as in Fig. 1. A chromosome (arrows) fails to recruit Cnp1 and remain unsegregated. (**f**) Series of frames from films of cells undergoing meiosis. Tubulin and histone H3 are observed as in Fig. 1. Scale bars in **e,f** represent 5 μm. The arrow indicates a chromosome that fails to segregate at MI and MII.

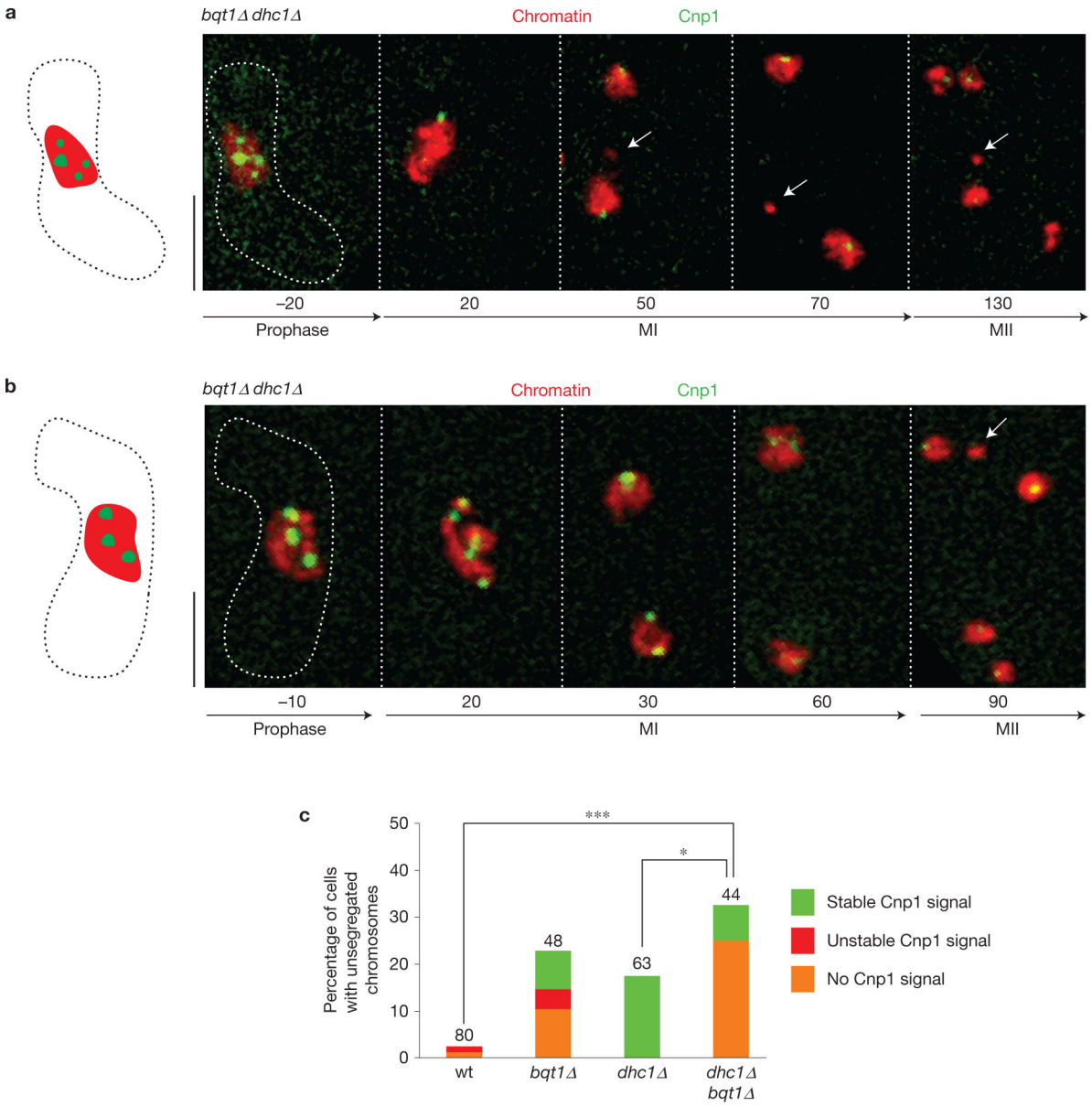

Figure 4.

Impaired kinetochore assembly is not a result of horsetail movement or reduced meiotic recombination. Cnp1–chromatin association was assessed as in Fig. 2 in cells lacking Dhc1, which is required for robust meiotic prophase nuclear ('horsetail') movements. In *dhc1Δ* meiocytes, bouquet formation occurs but levels of meiotic recombination are reduced. (**a,b**) Series of frames from films of cells undergoing meiosis. Cnp1 and chromatin were assessed as in Fig. 2. These examples show *dhc1Δ bqt1Δ* cells with chromatin masses failing to attach to the spindle and lacking a stable Cnp1–GFP signal (arrows). Numbers below frames represent minutes before or after MI. Scale bars represent 5 μm. (**c**) Quantification of Cnp1 localization. For each genetic background, the percentage of cells harbouring unsegregated chromosomes is plotted; the superimposed colour code specifies the pattern of Cnp1–GFP signal in those cells. See Methods for definitions of stable and unstable. Number of cells

filmed is indicated above each bar. (wt–*bqt1Δ dhc1* $P = 0.0001$, *bqt1Δ dhc1Δ*-*dhc1Δ* $P = 0.04$, see Methods for details). In *dhc1Δ* meiocytes, all unsegregated chromosomes show a stable Cnp1–GFP focus. In *dhc1Δ bqt1Δ* meiocytes, a subset of centromeres remain associated with the SPB throughout meiotic prophase. However, the occurrence of unsegregated chromatin masses lacking Cnp1–GFP is not suppressed.

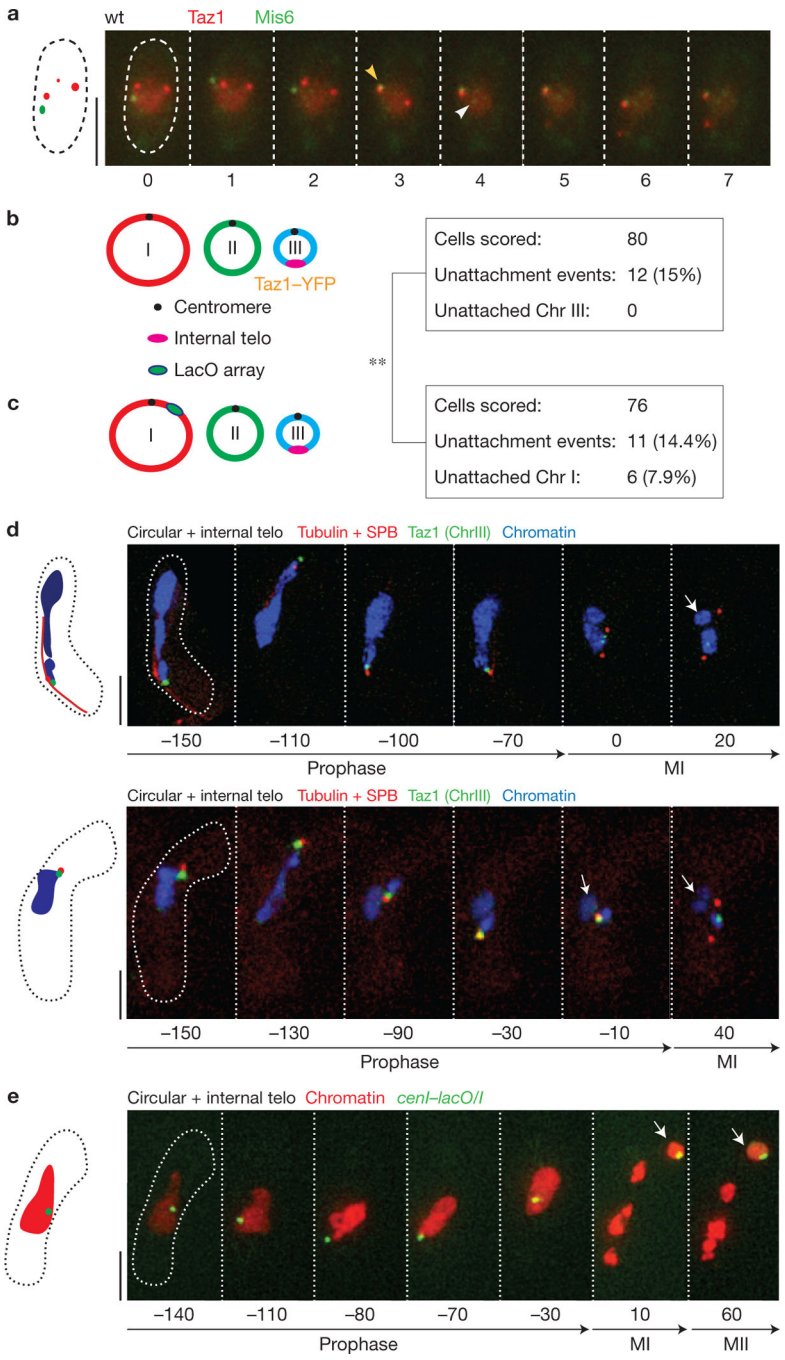

Figure 5.

Proximity to telomeres promotes meiotic centromere assembly. (**a**) Telomeres and centromeres co-localize at the onset of meiotic prophase. Azygotic meiotic cells (used to increase the synchrony of the meiotic culture) were filmed every 18 s. Centromeres and telomeres were visualized via endogenously tagged and functional Mis6–GFP and Taz1–mCherry, respectively. Yellow arrowhead indicates telomere–centromere co-localization and white arrowhead indicates the release of a subset of centromeres from the SPB. (**b**) Chromosomes associated with the bouquet are protected from centromere assembly defects.

Left: diagram of genome assessed for chromosome–spindle attachment failures. Each of the three chromosomes has circularized. The pink ellipse on Chr III represents an internal telomere repeat tract that is visualized via bound Taz1–YFP. Right: quantification of unattached chromosomes. Unsegregated chromosomes (Chr I and Chr II) are observed in 15% of cells, but the chromosome harbouring the internal telomere (Chr III) is never unsegregated. (**c**) Chromosomes not associated with the telomere bouquet suffer centromeric defects. Left: the centromere of Chr I is visualized *via cenI–lacO/I* (green ellipse) and Chr III harbours the internal telomere stretch. The internal telomere stretch on Chr III fails to protect centromeres on Chr I or Chr II. Right: quantification of unattached chromosomes. Segregation rates for Chr III and Chr I (comparing **b** and **c**) differ significantly (P =0.006, see Methods). (**d**) Series of frames from films of meiocytes scored in **b**. Cells harbour endogenously tagged and functional alleles of Taz1 and Sid4 (a SPB protein), as well as tagged tubulin and histone H3 as in Fig. 1. Numbers below frames represent minutes before or after MI. Scale bars represent 5 μm. Unsegregated chromosomes (white arrows) do not show Taz1 signal. (**e**) Series of frames from a representative film of circular +internal telo cells undergoing meiosis, as scored in **c**. Chr I is observed via *cenI–lacO/I*; tubulin (*Atb2*) and histone H3 observed as in Fig. 1. Numbers below frames represent minutes before or after MI. Scale bars represent 5 μm. The two Chr I homologues (white arrow) have failed to attach to the spindle.

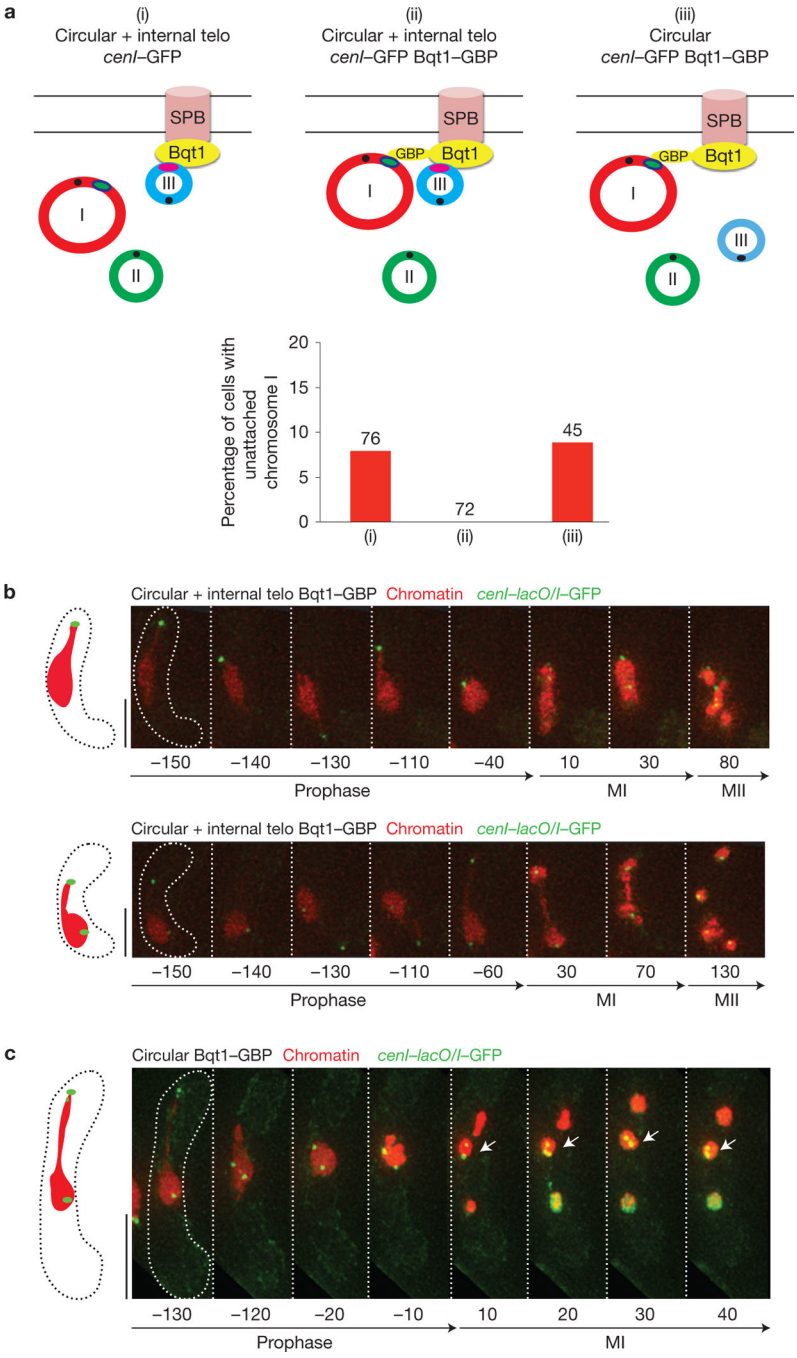

Figure 6.

Centromeres recruited to the bouquet microenvironment are protected from assembly defects. (**a**) (i)–(iii) Diagrams of genomes assessed for segregation defects. (i) The centromere of Chr I is visualized via *cenI–lacO/I* (green ellipse, as in Fig. 5c) and Chr III harbours the internal telomere stretch that localizes to the SPB during prophase. (ii) The centromere of Chr I is recruited to the SPB by binding of LacI–GFP to Bqt1–GBP (see text). In addition, Chr III harbours the internal telomere stretch and therefore localizes to the SPB. (iii) Chr I is recruited to the SPB by binding to the Bqt1–GBP fusion protein (see text). Chr

III lacks telomeric repeats, and is therefore away from the SPB. The graph shows quantification of Chr I segregation defects for each scenario diagrammed. Recruitment of *cenI* to the SPB during prophase confers protection from failed spindle attachment if the internal telomere is also present at the SPB; if the internal telomere is absent, protection fails despite tethering of Chr I to the SPB. Number of cells filmed is indicated above each lane. (**b**) Series of frames from representative films of circular + internal telo meiocytes (scored in (ii)). Chr I is observed via *cenI–lacO/I* (as in Fig. 5) and histone H3 is observed as in Fig. 1. Note the recruitment of ChrI (green dot) to the SPB (end of the chromatin streak), and the subsequent attachment of the chromosomes to the spindle. Numbers below frames represent minutes before or after MI. Scale bars represent 5 μm. MII in 'circular' strains is difficult to visualize clearly because entangled chromatin masses quickly collapse onto each other on spindle dissolution. (**c**) Series of frames from representative films of 'circular' cells scored in (iii) undergoing meiosis. Chr I is observed via *cenI–lacO/I* (as in Fig. 5) and histone H3 is observed as in Fig. 1. Numbers below frames represent minutes before or after MI. Scale bars represent 5 μm. Note the recruitment of Chr I (green dot) to the SPB (end of the chromatin streak); however, as no telomere stretch co-localizes to the SPB, centromere I fails to attach to the spindle.

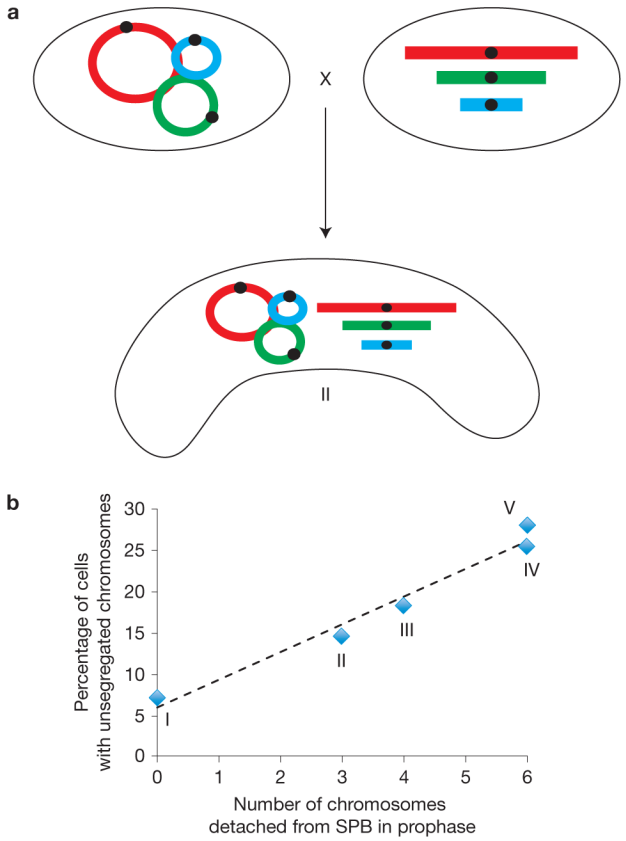

Figure 7.

Linear correlation between number of telomeres participating in the bouquet and centromere attachment capability. (**a**) Mating of a strain harbouring circular chromosomes with a wt strain yields a meiocyte in which three (linear) chromosomes associate with the bouquet and three (circular) chromosomes do not. This meiocyte corresponds to point II in **b**. (**b**) Positive linear correlation between the number of chromosomes devoid of telomeres attaching to the SPB in a given cell and the percentage of cells with a nonfunctional centromere. Five strains were scored: (I) meiocytes derived from mating wt strains (all chromosomes participate in the bouquet; therefore, no chromosomes are detached from the SPB, $n=87$); (II) meiocytes depicted in a, harbouring three linear (telomere-containing) and three circular (telomere-less) chromosomes ($n = 82$); (III) meiocytes derived from mating two circular + internal telo strains (see text) of opposite mating type (only two chromosomes participate in the bouquet; therefore, four chromosomes are detached from the SPB $n = 94$); (IV) as in III, but with deletion of *bqt1+*, which abrogates binding of the internal telomere to the SPB (no telomeres participate in the bouquet; therefore, six chromosomes are detached from the SPB, $n = 55$); (V) cells from mating of two circular chromosome-containing strains entirely lacking telomere sequences (no telomeres participate in the bouquet and therefore 6 chromosomes are detached from the SPB, $n =25$). The dashed line is a linear fit, $R^2 =0.87$.

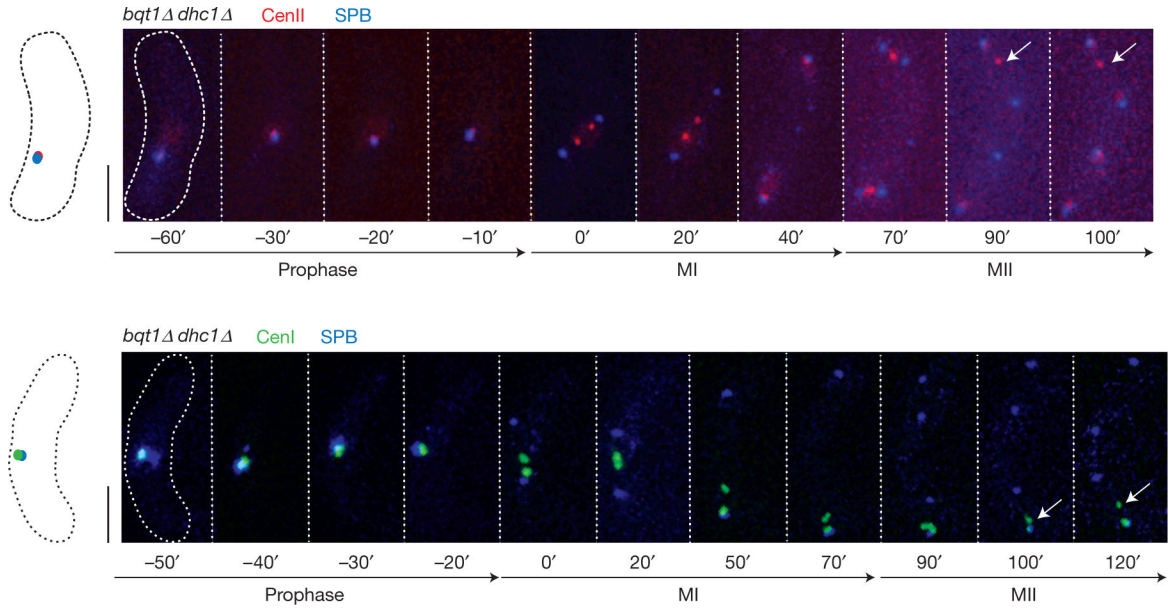

Figure 8.

Impaired kinetochore function at centromeres that localize to the prophase SPB without the presence of telomeres. Series of frames from films of cells undergoing meiosis. Endogenously tagged Sad1–CFP (which localizes to the SPB, blue) is observed along with centromere II (red, visualized via *cenII–tetO/R*) or centromere I (green, visualized via *cenI-lacO/I*). Numbers below frames represent minutes before or after MI. Scale bars represent 5 μm. Note co-localization of centromere and SPB throughout prophase, and the subsequent non-attachment phenotype of *cenII* or *cenI* (arrows).